Journal of Marine Systems 154 (2016) 157–171

Contents lists available at ScienceDirect

Journal of Marine Systems

journal homepage: www.elsevier.com/locate/jmarsys

Impacts of a 4-dimensional variational data assimilation in a coastal ocean model of southern Tyrrhenian Sea

I. Iermano [a,*], A.M. Moore [b], E. Zambianchi [a,c]

[a] Dipartimento di Scienze e Tecnologie, Università degli Studi di Napoli "Parthenope" and CoNISMa, Napoli, Italy
[b] Department of Ocean Sciences, University of California, 1156 High Street, Santa Cruz, CA 95064, United States
[c] Istituto di Scienze dell'Atmosfera e del Clima, Consiglio Nazionale delle Ricerche, UOS Roma, Italy

ARTICLE INFO

Article history:
Received 2 July 2015
Received in revised form 28 September 2015
Accepted 30 September 2015
Available online 30 October 2015

Keywords:
Coastal oceanography
Ocean modeling
Data assimilation
Variational methods
HF radars

ABSTRACT

The impact of the assimilation of satellite sea surface height, sea surface temperature and surface velocity fields observed by a set of high-frequency (HF) radars is studied using a three-dimensional ocean circulation model configured for the southern Tyrrhenian Sea. The study period is October–December 2010 covered by a large number of data. The nonlinear model is based on the Regional Ocean Modeling System (ROMS) and the data assimilation component on the four-dimensional variational (4D-Var) algorithm.
Assimilation proceeds in a series of 7-day windows, providing an analysis solution in each window.
The assimilation of surface velocity combined with other observations has more utility in recovering the density fields based on the theory of geostrophic adjustment and a strong impact both on near-surface horizontal volume fluxes and subsurface flows, constraining surface geostrophic currents in the area not covered by the HF radar data.
The adjoint of the 4D-Var gain matrix was used to quantify the impact of individual observations and observation platforms on different aspects of the 4D-Var circulation estimates during both the analysis and subsequent forecast cycles. In this study, we focus on the alongshore transport of the surface and intermediate waters in the eastern zone of southern Tyrrhenian Sea. The majority of the observations available during any given analysis cycle are from HF radar, and on average these data, together with SSH data, exert the largest controlling influence on the analysis increments of coastal transport. Also, observations from satellite platforms in the form of SST have a considerable impact on analyses and forecasts of coastal transport, even though these observations represent a relatively small fraction of the available data at any particular time.
During 4D-Var, the observations are used to correct for uncertainties in the model control variables, namely, the initial conditions, surface forcing, and open boundary conditions. It is found that correcting for uncertainties in the initial conditions and only secondarily in the boundary conditions has the largest impact on the analysis increments in alongshore transport.
Finally, we note that both the control vector and the observation impact calculations are a useful way for monitoring the performance of the data assimilation system, as well as quantifying the impact of the observations on the circulation estimates.

1. Introduction

State-of-the-art numerical ocean models are widely used in coastal oceanography to simulate the three-dimensional circulation of limited area domains for studies of regional ocean dynamics, biogeochemistry, geomorphology, and ecosystem processes.

When operated as real-time now-cast or forecast systems, these models offer predictions that assist decision makers on issues related to water quality and public health, coastal flooding, shipping, maritime safety, and other applications. The dynamic ocean state estimate provided by ocean circulation models critically depends on the model boundary conditions, as well as on its capability to resolve the water parameters, both spatially and temporally.

However, research and development in technology over the last three decades have substantially improved coastal ocean observing systems, e.g. by buoys, satellites, moorings, coastal radars, etc. These advanced ocean observing systems now provide a large volume of ocean measurements in real-time, addressing the traditional "scarcity" of observational data in oceanography.

The increasingly available ocean observations are appropriate for establishing "data assimilation" (hereafter DA) approaches, a series of mathematical techniques of growing complexity in which observational

* Corresponding author at: Dipartimento di Scienze e Tecnologie (DiST), Università "Parthenope", Centro Direzionale, Isola C4, 80143, Napoli, Italy.
E-mail address: ilaria.iermano@uniparthenope.it (I. Iermano).

http://dx.doi.org/10.1016/j.jmarsys.2015.09.006
0924-7963/

data are dynamically combined with numerical models in order to obtain the best representation of the ocean state. The use of complex DA approaches provide better results with respect to those obtained by using only the numerical model or by analyzing the observational data alone (Anderson et al., 1996). The key point about DA techniques is that oceanic observations are sparse and numerical models are limited in accuracy; but if taken together, they may yield a quantitative description of the state of the ocean that is superior to either models or data alone.

DA can be used at different scales and in various applications to integrate diverse available data sets with dynamical models in order to perform more accurate process studies; to provide a foundation for hypothesis testing and model improvement, including estimating model and data errors (uncertainty modeling); to initialize ocean models, or the ocean component of coupled models, and assimilate subsequent observations for optimal forecasting; to estimate model parameters and parameterizations, including forcing and lateral boundary conditions, and provide the means to assess observing systems, measure the usefulness of new data, and collect the most useful observations through adaptive sampling; eventually, to obtain a better understanding of the ocean.

The assimilation of satellite-derived data can be considered nowadays as an advanced and widespread activity (e.g. Dombrowsky et al., 2009; Lellouche et al., 2013; Pinardi and Coppini, 2010), even in coastal regions of the Mediterranean Sea, as demonstrated by the works of Vandenbulcke et al. (2006) in the Gulf of Lions, Korres et al. (2009) in the Aegean Sea, and Olita et al. (2012, 2013), respectively, in the Sicily Channel and in the western Sardinian Sea.

In particular, there is a large body of literature dealing with assimilation of satellite data using variational techniques. The time-dependent variational method is one DA approach largely applied to studies of ocean variability on regional and coastal scales, as demonstrated by various works in literature. Hoteit and Köhl (2006) applied an adjoint data assimilation in the eastern subtropical North Atlantic using in situ and satellite data as constraint. Powell et al. (2008) presented the theory and application results of the incremental 4DVAR assimilation method in ROMS in the Intra-Americas Sea using remotely sensed surface observations including sea surface temperature (SST) and sea surface height (SSH).

Other regional applications of variational technique are those of Broquet et al. (2009a) to the California Current System as well as the work of Chao et al. (2009); Kuparov et al. (2009, 2011) to a coastal ocean model off the western coast of the U.S; Zhang et al. (2010) to a coast domain in the center of the Mid-Atlantic Bight; Janekovic et al. (2013) to a coastal domain of Hawaiian islands.

The assimilation of velocity data is a recent phenomenon and is still evolving, although radar observational systems are potentially one of the most important data sets for coastal ocean state estimation (Paduan and Washburn, 2013).

One of the earliest DA studies using high-frequency (hereafter HF) radar data was reported by Lewis et al. (1998) for the Monterey Bay, CA, in which a pseudo-shearing stress, defined as the difference between the model surface current and HF radar data, was used to correct the model wind forcing. Breivik and Sætra (2001) reported HF radar surface current assimilation into a realistic coastal model for the Norwegian coast using an optimal interpolation (OI) method. An HF radar DA study for the Oregon coast was reported by Oke et al. (2002b), which used a sequential OI scheme based on the physical-space statistical analysis system (PSAS), and a time-distributed averaging procedure (TDAP). A representer-based 4-dimensional variational method (4D-Var) (Bennett, 2002) was used by Kurapov et al. (2003) to assimilate HF radar data into a simplified ocean model. Paduan and Shulman (2004) assimilated HF radar data using a PSAS scheme based on data-dependent velocity covariance functions in the Monterey Bay, CA.

Assimilation of HF radar data using a melding/nudging approach was reported by Wilkin et al. (2005) for the New Jersey inner-shelf. Barth et al. (2008) assimilated HF radar surface currents in the West Florida shelf using an ensemble-based error covariance method. Li et al. (2008) have used a three-dimensional variational assimilation (3D-Var) of HF radar data in the Southern California on an operational basis. A 4D-Var method was used by Hoteit et al. (2009) to assimilate HF radar data in the San Diego coastal region. More recently, Shulman and Paduan (2009) reported assimilation of HF radar-derived radial/total surface currents using PSAS scheme for the Monterey Bay, CA. In Gopalakrishnan and Blumberg (2012), a surface current observation system based on HF radar has been developed for the Raritan Bay, NJ, and the coastal waters of New York and New Jersey. The impact of the HF radar DA is analyzed by computing the DA skill by comparing (non-assimilated/assimilated) model solutions with *in situ* observations of three-dimensional currents, temperature, and salinity which have not been included in the assimilation.

In Yu et al. (2012), the impact of assimilation of sea surface velocity fields observed by a set of HF radars was studied using a three-dimensional ocean circulation model configured along the Oregon coast. The nonlinear model was based on the ROMS and the DA component on a system utilizing the representer-based variational algorithm.

Among the Italian coastal zones, the Gulf of Naples (hereafter GoN), and the surrounding area of the southern Tyrrhenian Sea, represent a particularly interesting area that is influenced by numerous environmental, socio-economic, and interacting cultural factors (strong anthropogenic impact, intense maritime traffic, the presence of the polluted Sarno River, tourist and economic activity, and four protected areas). Thus, pollutant release in this basin may have serious consequences in terms of the environmental sustainability and management of the coastal area.

For these reasons, a comprehensive understanding of the coastal circulation in this basin is of fundamental importance for proper planning and management of the coastal area and for the maintenance and improvement of environmental quality in the GoN.

The peculiar dynamics of the GoN qualify the region as a natural challenging laboratory for testing the skill of coastal ocean models and data assimilation methodologies.

Here we proceeded to implement a limited area ROMS (Shchepetkin and McWilliams, 2005) model in the southern Tyrrhenian Sea and a 4-dimensional variational data assimilation system was applied in the model domain using HF radar data, satellite sea surface height (SSH), and surface temperatures (SST).

The expected goal of this study was to assess the effects of the HF radar data, together with surface data coming from satellite in the form of SST and SSH on a coastal modeling system of the GoN area and surroundings.

In particular, we focus here on the impact of the observations on the 4D-Var circulation which is one of the many capabilities of the ROMS 4D-Var system (Moore et al., 2011c).

As described in Moore et al. (2011c), the observation impact calculations can be used to quantify the contribution of each individual datum to the difference between the background (or prior) and the analysis (or posterior) of some aspect of the ocean circulation and can also demonstrate the influence of initialization shocks on the circulation that are associated with each individual observations.

The observation impact calculations presented here are based on an adjoint approach and utilize the property of adjoint operators for identifying the subspace of the model state vector that is activated by the observations. While adjoint-based methods have been used previously in oceanography in attempts to identify optimal observing locations and observation types (e.g. Köhl and Stammer, 2004; Zhang et al., 2010), our focus here is on the impact of existing observations on estimates of the ocean circulation, following the approach originally developed in meteorology by Langland and Baker (2004), Daescu (2008), Zhu and Gelaro (2008), and Gelaro and Zhu (2009) and in oceanography by Moore et al. (2011c).

Our primary focus is the winter circulation in the vicinity of a coastal area of the southern Tyrrhenian Sea (namely, the Campania region

coasts and the Gulf of Naples), which is related to the circulation of the southern and mid-Tyrrhenian Sea (Buffoni et al., 1997) and also strongly affected by the local wind stress (Cianelli et al., 2015; Grieco et al., 2005; Iermano et al., 2012).

In the Tyrrhenian Sea, a basin-wide cyclonic circulation at all depths is present during winter, characterized by a northeastward flow of Levantine Intermediate Water (LIW) entering the Western Mediterranean through the Sicily channel, combined with a flow of modified AW coming from the Sardinia channel, which then roughly follows the same cyclonic motion (e.g., Astraldi and Gasparini, 1994; Krivosheya and Ovchinnikov, 1973; Millot, 1987).

A first good dynamical indicator of the autumn/winter circulation changes is the alongshore transport across a single section, and we use this indicator here to demonstrate how the available observations contribute to modify the coastal circulation via data assimilation during a specific period of the year. As a consequence, and with the aim generalizing the results obtained through the use of a single section, as well as to focus on the coastal area of the GoN and its surroundings, the average transport of the intermediate water LIW in a restricted coastal region of the model domain was also considered. The LIW transport has proved to be an important and dynamically relevant aspect of the circulation in the study area to assess the impacts of the data assimilation.

A brief summary of the ROMS model and 4D-Var configuration as well as the sequential strong constraint 4D-Var experiment set-up presented here and the dataset of observations used is presented in Section 2. The results of the experiments are presented in detail in Section 3: an assessment of the surface features together with the impact of observations on the coastal transport during each assimilation cycle is presented in Sections 3.1 and 3.2. Section 3.3 considers the impact of the assimilation on subsurface and deep layers. A summary of important results and conclusions is presented in Section 4.

2. Model configuration and experimental set-up

ROMS is a three-dimensional, free-surface, terrain-following ocean model that solves the Reynolds-averaged Navier–Stokes equations using the hydrostatic vertical momentum balance and Boussinesq approximation (Haidvogel et al., 2000; Shchepetkin and McWilliams, 2005). The governing dynamical equations are discretized on a vertical coordinate that depends on the local water depth. The horizontal coordinates are orthogonal and curvilinear allowing Cartesian, spherical, and polar spatial discretization on an Arakawa C-grid. The dynamical kernel includes accurate and efficient algorithms for time-stepping, advection, pressure gradient (Shchepetkin and McWilliams, 2003), several sub-gridscale parameterizations (Warner et al., 2005) to represent small-scale turbulent processes at the dissipation level, and various bottom boundary layer formulations to determine the stress exerted on the flow by the bottom.

ROMS is an open-source, ocean community-modeling framework supporting three different 4D-Var data assimilation methodologies: a primal form of the incremental strong constraint 4D-Var (I4D-Var), a strong/weak constraint dual form of 4D-Var based on a Lanczos formulation of the augmented Restricted Preconditioned Conjugate Gradient (RPCG) algorithm, and a strong/weak constraint dual form of 4D-Var based on the indirect representer method (R4DVar) (Gürol et al., 2013; Moore et al., 2011a,2011b).

Our model domain covers the GoN and the adjacent open sea region extending between 39°–42°N and 12°–16°E with 3 km horizontal resolution and 30 terrain-following vertical levels (Fig. 1).

The model forcing was derived from the global reanalysis output of the Era Interim dataset (Dee et al., 2011) from the European Centre for Medium-Range Weather Forecasts (ECMWF). The ocean surface fluxes were derived using the bulk formulations of Fairall et al. (1996), and represent the background (or prior) surface forcing in the incremental formulation of 4D-Var.

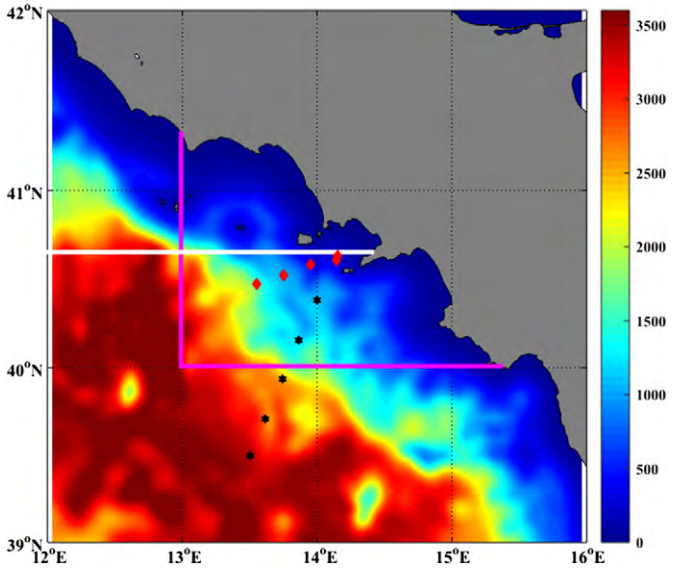

Fig. 1. ROMS model domain and bathymetry. The section at 40.5°N as well as the coastal area considered for the calculation of meridional transports are indicated in white and magenta, respectively. The locations of CTD stations (TYR and GON sections in black and red, respectively) are shown for reference.

The model domain has open boundaries at the northern, southern, and western edges, and at these boundaries, the tracer and velocity fields were prescribed, while the free surface and vertically integrated flow were subject to Chapman (1985) and Flather (1976) boundary conditions, respectively.

The time evolving prescribed open boundary solution was taken from the daily updated High Resolution Atlantic and Mediterranean Mercator Ocean dataset product (Lellouche et al., 2013), with a resolution of 1/12°, and represents the background (prior) boundary conditions in the incremental formulation of 4D-Var.

Prior to DA, the underlying numerical ROMS model was tested with respect to its skill in simulating the observed ocean structure, understanding multi-scale interactions, inferring and modeling the effects of larger scales in smaller-scale simulations, comparing the benefits of enhanced model resolution and model physics to those of enhanced estimation methods.

The efficacy of the model without DA has been explored by way of model-data comparisons using in particular HF radar data to show that the nested model reproduces variability on the shelf qualitatively correctly (Cianelli et al., 2015).

This activity is fundamental for model improvement and is a necessary element of a robust assessment of DA efforts.

Even if our model implementation of southern Tyrrhenian Sea is nested in a coarse, global product in which available observations are already assimilated, and for that reason, the information it brings is transferred to our local model through initial and boundary conditions, there is the necessity to assimilate data also in the high-resolution model.

As discussed in Vandenbulcke et al. (2006), when observations are assimilated in a regional model, they have a positive impact on the solution. Even supposing that the global model is approximately correct, a higher-resolution regional model is generally superior when corrected using observations and data assimilated, rather than relying solely on the transfer of information from the global model.

The starting point for the ROMS/4D-Var experiments presented here was taken from an interannual run performed without any data assimilation from the year 2007 to 2010. Strong constraint incremental 4D-Var was performed sequentially starting on 1 October 2010, using 7-day assimilation windows and iteratively adjusting the model initial conditions, surface forcing, and open boundary conditions.

HF radar data together with satellite data were assimilated into the high-resolution implementation of coastal model, and the DA analysis solution during each assimilation window was compared against the unassimilated model solution.

To evaluate the impact of 4D-Var data assimilation, two identical experiments are compared : a simulation considered as control run, which is part of the interannual run from 2007 to 2010 with no DA (hereafter called free-run), and a DA solution (hereafter called analysis) assimilating satellite data and surface velocities. The analysis and control experiments have the same initial conditions at the first day (1 October 2010) of assimilation, therefore they are identical with the exception of the DA.

2.1. Observations

The observations assimilated in the model were collected from various different instruments and satellite platforms and included the data described in the following sections.

2.1.1. HF radar-derived surface velocities

The GoN is one of the very few sites along the Italian coast that benefits from the availability of real-time surface velocity data provided by a system of HF coastal radars (Bellomo et al., 2015; Corgnati et al., in press).

In 2004, the first core of a network of HF coastal radars was installed in the GoN, permitting the real-time, synoptic monitoring of the surface current field at the basin scale (Fig. 2). This system has been operated by the former Department of Environmental Sciences, now Department of Science and Technology, of the Università degli Studi di Napoli "Parthenope" on behalf of the Centre for the Analysis and Monitoring of Environmental Risk (AMRA Scarl). The system installed in the GoN is a SeaSonde type manufactured by CODAR Ocean Sensors (Mountain View, California, USA). It operates in the 25 MHz band, measuring surface currents relative to the upper 1 m of the water column. The temporal resolution of the system is 1 h, while the range is approximately 35 km from the coast. The original network installed in 2004 comprised two remote stations (in Portici and in Massa Lubrense); in this configuration, the spatial resolution was 1250 m (Menna et al., 2007). In 2008, a third antenna has been installed in Castellammare di Stabia; this implementation improved both the spatial coverage and resolution (1000 m) and the system data quality has been thoroughly validated (see, e.g., Uttieri et al., 2011).

2.1.2. Sea surface temperature data

The sea surface temperature (SST) product used is a merged data set derived from both microwave and infrared sensors carried on multiple platforms and provided by the NOAA OceanWatch catalog (http://oceanwatch.pfeg.noaa.gov/thredds/catalog.html). The microwave instruments can measure ocean temperatures even in the presence of clouds, though the resolution is relatively coarse when considering features typical of the coastal environment. These data are complemented by the relatively fine measurements of infrared sensors.

Blended SST measurements, gathered by Japan's Advanced Microwave Scanning Radiometer (AMSR-E) instrument, a passive radiance sensor carried aboard NASA's Aqua Spacecraft, NOAA's Advanced Very High Resolution Radiometer, NOAA Geostationary Environmental Satellites (GOES) Imager, and NASA's Moderate Resolution Imaging Spectrometer (MODIS), were available from November 2006 every day as a 5-day mean product with horizontal resolution 10 km. The latter were merged with SST data from NASA's Terra Spacecraft provided by NOAA CoastWatch, and gathered by the MODIS, currently supporting only daytime imagery. Data were available from March 2000 every day as an 8-day mean product with horizontal resolution 4.4 km.

2.1.3. Aviso absolute dynamic topography

ADT combines sea level anomaly data (a merged product composed of SSALTO-Duacs data from TOPEX/Poseidon, Jason-1&2, Envisat, ERS-1&2, and GFO measurements on a reference period based on a 20-year [1993–2012] period (Pujol et al., 2013) and the mean dynamic topographic data estimated by Rio et al. (2013), provided by Aviso and the Centre National d'Etudes Spatiales (CNES). Data are available every day with horizontal resolution 1/8° over the whole Mediterranean Sea (ftp://ftp.aviso.altimetry.fr/regional-mediterranean/delayed-time/grids/madt/all-sat-merged/h).

ADT was compared to the model SSH for the DA period, and calibrated to ensure that the spatio-temporal mean of ADT and the free-run

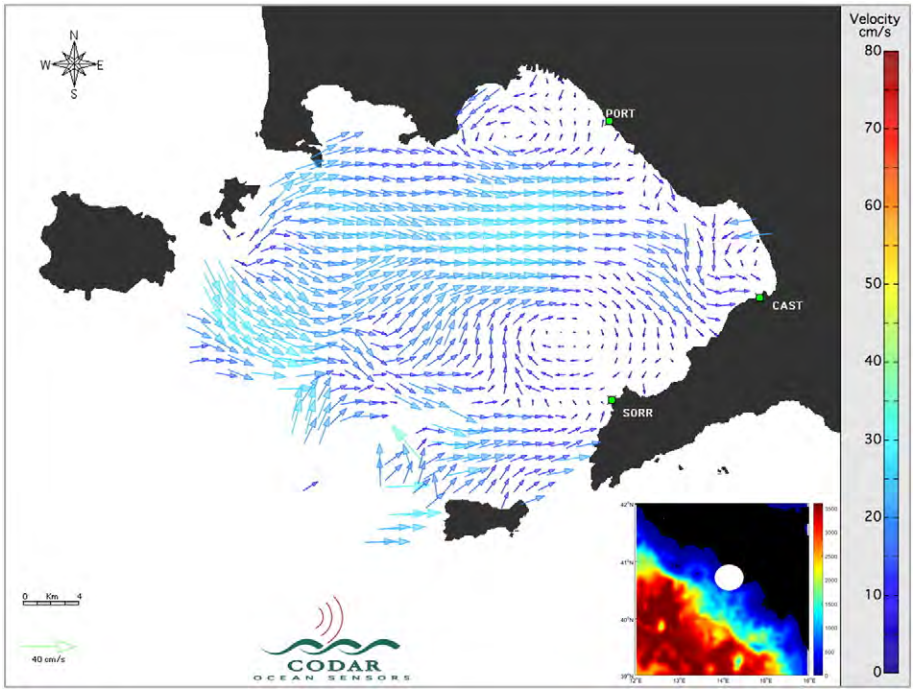

Fig. 2. Typical hourly surface current field of HF radar during the period of the DA experiment, showing its coverage and the model grid (inset).

model are equal. The calibration takes the form of a mean offset to ADT which is constant in space and time. The procedure for computing SSH for assimilation basically started from the space and time mean of ADT over the whole domain, then the same procedure was repeated using the free-run experiment spanning the same period as the Aviso observations. The observed space–time mean of ADT from Aviso data was removed and replaced with the space–time mean of the ROMS model.

2.2. 4D-Var configuration

If we denote by $\mathbf{z}$ the control vector composed of the initial conditions, surface forcing, and open boundary conditions, then incremental 4D-Var proceeds by minimizing the cost function given by:

$$J = \delta \boldsymbol{z}^T D^{-1} \delta \boldsymbol{z} + (\boldsymbol{G}\delta \boldsymbol{z} - \boldsymbol{d})^T \boldsymbol{R}^{-1} (\boldsymbol{G}\delta \boldsymbol{z} - \boldsymbol{d}) \quad (1)$$

where $\delta \mathbf{z} = \mathbf{z} - \mathbf{z_b}$ is the control vector increment and $\mathbf{z_b}$ is the background control vector; $\mathbf{D}$ is the *prior* error covariance matrix; $\mathbf{d} = \mathbf{y}^o - H(\mathbf{z_b})$ is the innovation vector where $\mathbf{y}^o$ is the vector of observations; $\mathbf{R}$ is the observation error covariance matrix; H is the observation operator that maps $\mathbf{z_b}$ to the observation points; and $\mathbf{G}$ is the tangent linearization of H. The increment $\delta \mathbf{z}$ that minimizes J is identified using a truncated iterative Gauss–Newton method involving sequences of inner- and outer-loops (Moore et al., 2011a).

Before running ROMS 4D-Var, it is necessary to specify the background error covariance $\mathbf{D}$ for the initial conditions, surface forcing, and open boundary conditions and the observation error covariance matrix, $\mathbf{R}$ (Moore et al., 2011a,2011b). In this section we will summarize the choice of parameters for $\mathbf{D}$ and $\mathbf{R}$.

Observation errors were assumed to be uncorrelated in space and time, resulting in a diagonal observation error covariance matrix, $\mathbf{R}$. The variances along the main diagonal of $\mathbf{R}$ were assigned as a combination of measurement error and the error of representativeness.

Measurement errors were chosen independent of the data source, with the following standard deviations: 0.07 m s^{-1} for HF radar components, 0.4 °C for SST, and 0.02 m for ADT.

The background error standard deviations for the unbalanced initial condition components of the control vector were estimated based on the variance of the model run for the period 2007–2010 subject only to surface forcing (i.e. no data assimilation).

Following Broquet et al. (2009a, 2011), the climatological standard deviation for each calendar month was computed from the model run for each component of the state vector at every grid point (Moore et al., 2011a), and these standard deviations used as the background error standard deviations during the appropriate month of each assimilation cycle.

The temporal variability of the ECMWF surface forcing for the period 2007–2010 was used as the variance for background surface forcing error, and the open boundary condition background error variances were chosen to be the variances of the Mercator Ocean fields at the boundaries.

The decorrelation length scales used to model the background errors of all initial condition control variable components of $\mathbf{D}$ were 50 km (for the free surface and tracers) and 30 km (for the 2D and 3D momentum components) in the horizontal and 30 m in the vertical. Horizontal correlation scales chosen for the background surface forcing error components of $\mathbf{D}$ were 100 km both for the wind stress and for heat and freshwater fluxes. The correlation lengths for the background open boundary condition error components of $\mathbf{D}$ were chosen to be 50 km (for the free surface and tracers) and 30 km (for the 2D and 3D momentum components) in the horizontal and 30 m in the vertical.

The surface forcing and boundary condition of the increments $\delta \mathbf{z}$ were computed daily, and interpolated to each intervening model time step.

2.3. Sequential strong constraint 4D-Var and experimental set-up

In the experiments presented here, ROMS 4D-Var was run sequentially for the period October–December 2010. Because of the uncertainty in assigning model error, all experiments presented here assume the strong constraint, although there is nothing to preclude the same computations using the weak constraint instead (i.e. accounting for model error; Moore et al., 2011a).

In all cases, the control vector $\delta \mathbf{z}$ was composed of increments to the initial conditions, surface forcing, and open boundary conditions. The background initial conditions at the start of each assimilation cycle were chosen to be the analysis at the end of the previous assimilation cycle. The background surface forcing and open boundary conditions, however, are always those taken from the ECMWF and Mercator datasets, respectively (Section 2).

4D-Var was run with 1 outer-loop and 15 inner-loops spanning 7-day assimilation cycles when the cost function J can typically be reduced by a factor of about ~3 during each assimilation cycle (Broquet et al., 2009a,b, 2011; Moore et al., 2011b; Powell, et al., 2008).

Our focus here is on the circulation of the southern Tyrrhenian Sea, one of the major sub-basins of the Mediterranean Sea. It has a triangular shape and a very complex bathymetry and is connected to the other basins of the western Mediterranean Sea mainly through the Corsica Channel (north) and a broad opening between Sardinia and Sicily in the south (Rinaldi et al., 2010).

The fluxes through the straits of Sicily and Sardinia exert an important control on the circulation. Surface waters of Atlantic origin (AW) enter the Tyrrhenian Sea off the northern Sicilian coast and flow northeastward along the eastern boundary of the basin (Buffoni et al., 1997; Krivosheya and Ovchinnikov, 1973; Poulain and Zambianchi, 2007) following an overall cyclonic pattern, proceeding along the western coast of Italy and then entering the Ligurian Sea through the Corsica Channel (Rinaldi et al., 2010). This surface northward flow is present during the whole year but more evident during the winter (Astraldi and Gasparini, 1994; Buffoni et al., 1997) then returns southbound on the western side of the Sardinian Channel and forms a rather stable cyclonic gyre (Poulain and Zambianchi, 2007).

The challenge for 4D-Var here is to therefore build reliable estimates of the actual ocean conditions in this dynamic region, particularly during the winter season such as the period analyzed in the experiment.

In this case, most of the observations that were assimilated were collected in real-time from the HF radar system installed in the GoN and from satellite. The HF radar data are limited to a narrow region (Fig. 2) while the satellite observations are uniformly distributed in space and time across the region, which demonstrates the ability of 4D-Var to dynamically interpolate information from remotely sampled observations.

In order to quantify the impact of the available ocean observations and data assimilation on the circulation, we considered two measures of transport as quantitative indicators of the circulation changes that occur in the southern Tyrrhenian region due to assimilating the observations: the transport of surface waters (upper 500 m) across the section situated at 40.5°N; the average transport of the intermediate water between 300 and 600 m depth across a restricted coastal region of the model domain including the GoN and its surroundings. The latter captures a major pathway of LIW in this region. The section as well as the coastal area considered for the calculation of meridional transports are indicated in Fig. 1.

The observation impact calculations presented here can formally quantify the value of each observing platform during the analysis-forecast cycles and therefore provide quantitative information about the observability of the transports associated with the winter circulation, and the ability of 4D-Var to dynamically interpolate information from the observations through the model domain.

3. Results and discussion

3.1. Qualitative assessment of the surface features

The first evaluation of the quality of the analyses and the effect of the data assimilation was carried out through a qualitative comparison of the simulated features of the surface circulation with those detected by independent satellite observations in the form of MODIS chlorophyll-a data.

We evaluated the impact of the assimilation in terms of the change/improvement in the reproduction of surface features by comparing the surface analysis fields with synoptic observations provided by optical and infrared satellite images. In order to do this, MODIS AQUA and TERRA level-2 data of chlorophyll-a concentration were used to compare the footprints of mesoscale and submesoscale features with those of the numerical experiment with and without DA.

The dates selected for this comparison were based on the absence of cloud cover (limiting the optical and infrared satellite measurements) and on the ability to emphasize the differences between the experiments. Fig. 3c shows the daily average salinity fields of the free-run and 4D-Var analysis simulations for 14 November 2010 compared to the MODIS chlorophyll-a concentration field for the same date. In this case, we used an optical product instead of SST to ensure the independence of the data from the DA experiment used for this qualitative assessment.

The main differences are found in the behavior of the coastal salinity distribution, detected in the model results by salinity ranging from 37.5 to 38 psu. In the free-run simulation (Fig. 3a), the squirts and jets both in the GoN and its northern coastal area (from 13° to 14.5°E) are not visible, while they are recovered quite well in the 4D-Var analysis (Fig. 3b). The satellite image shows the clear signature of submesoscale anticyclonic meanders approximately located at 13°E and 41°N, in the GoN (14.25°E–40.6°N) and also further south (14.75°E–40.3°N). These signatures can also be observed in the 4D-Var analysis which clearly reveals that the coastal salinity signal is very accentuated and it extends for several kilometers offshore reaching almost the island group (13°E–41°N) at about 70 km from the coast.

The qualitative comparison of free-run and analysis simulations with independent synoptic satellite data indicates that 4D-Var data assimilation can recover some of the dynamical features, such as coastal squirts and meanders, in the GoN portion of the domain and its surroundings that are otherwise absent in the free-run.

3.2. Impact of the observations

The meridional transport across a section is used to better understand how and where the assimilation of satellite and HF radar data, which should provide information about the submesoscale and

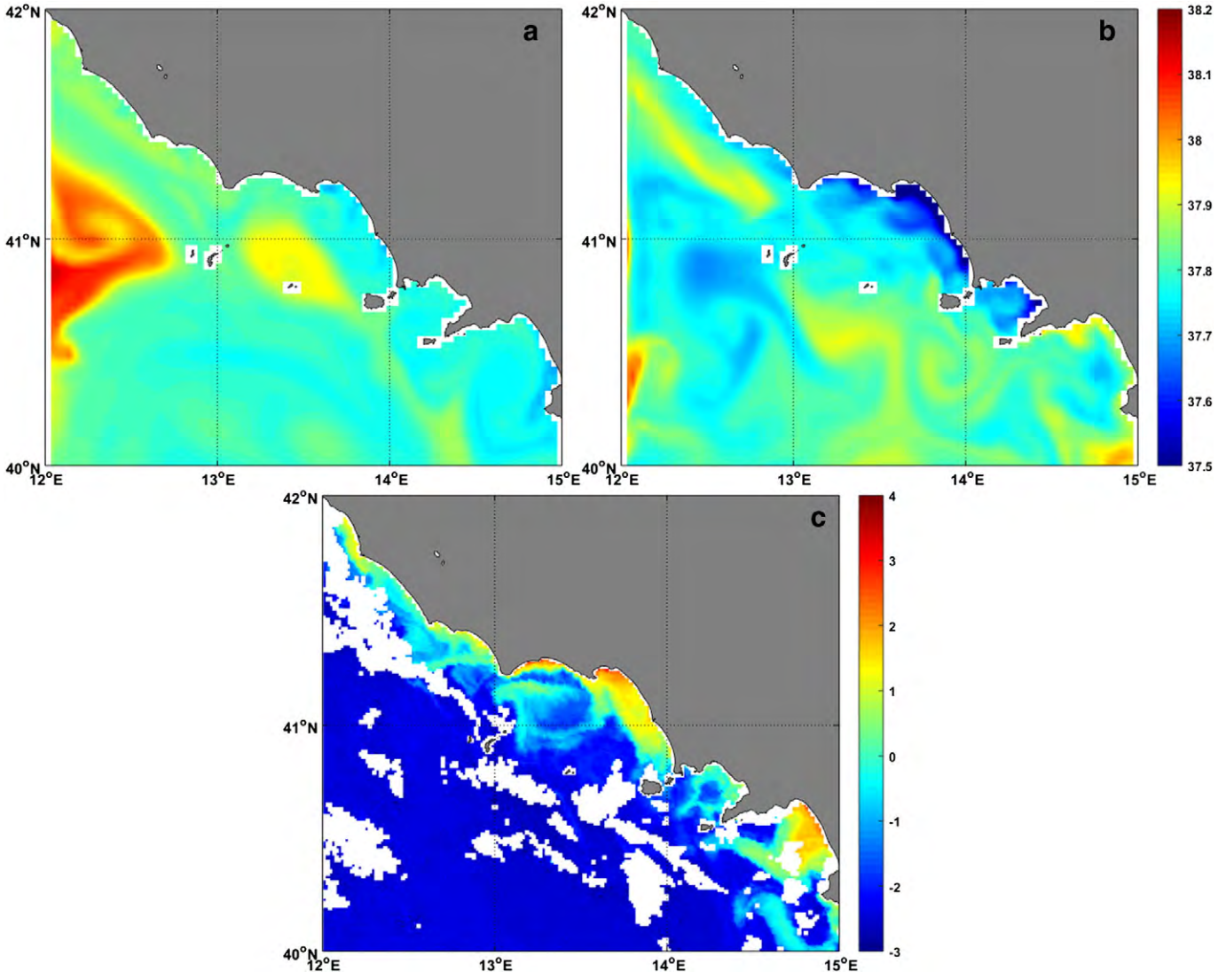

Fig. 3. Daily average salinity fields from the free-run and 4D-Var analysis simulations (a and b) for 14 November 2010 compared to the MODIS chlorophyll-a concentration field (c).

mesoscale circulation, can bring about important changes in the mean flow interactions.

The 7-day average transport across the section situated at 40.5°N latitude in the upper 500 m during each analysis cycle was considered and used here as a scalar circulation metric, denoted by I, to quantify the impact of each available ocean observation and data assimilation on the circulation. The transport section is indicated in Fig. 1.

Fig. 4a shows a time series of I_b at 40.5°N for the background circulation estimate for each 7-day 4D-Var cycle. In this case, the transport varies smoothly between 0.75 Sv southward at the beginning of experiment and 1.5 Sv northward at the end. The transport crossing the transect is generally northward with a mean of 0.3 Sv, a standard deviation of 0.7 Sv, and peak values during the beginning of winter of 1.5 Sv, although at the beginning of experiment (October) I is quite small.

The time averaged alongshore transport I_a of the 4D-Var analyses across the same section differs quite significantly from the background estimates I_b.

A time series of the transport increment $\Delta I = I_a - I_b$ during each assimilation cycle is shown in Fig. 4b. Two estimates of ΔI are shown:

In one case, the ΔI was computed directly from the difference between the analysis and background circulation estimates of the nonlinear ROMS (referred to as NLROMS), while in the other case, the ΔI were computed using the tangent linear assumption. As shown in Moore et al. (2011c), invoking the tangent linear assumption leads to

$$\Delta I = \boldsymbol{d}^T \boldsymbol{K}^T (\partial \mathrm{I} / \partial \delta z)\big|_{\boldsymbol{zb}}$$

where $\mathbf{K} = \mathbf{DG}^{\mathrm{T}}(\mathbf{GDG}^{\mathrm{T}} + \mathbf{R})^{-1}$ is the Kalman gain matrix.

The two time series generally agree well during most of the time period, indicating that the tangent linear assumption is valid during each 7-day assimilation cycle, although there is a significant discrepancy toward the end of November and beginning of December. However, at this time, the transport changes are small (but not necessarily $\delta \boldsymbol{z}$) at which times the tangent linear approximation is more susceptible to error. The mean of the alongshore transport increments of Fig. 4b is comparable to that of I_b in Fig. 4a.

The transport increments made by 4D-Var are largest at the beginning of the experiment and decrease over time.

The transport increments can be decomposed into the individual contributions from the 4D-Var the control variable increments for the initial conditions, surface forcing and open boundary conditions. Time series of the individual contributions to ΔI are shown in Fig. 5 for each 4D-Var cycle. Fig. 5 shows that there are clearly times when the increments in the initial conditions dominate, and times when the increments to the boundary conditions are the primary factor controlling ΔI across 40.5°N. During some cycles, the changes in ΔI associated with the increments in the initial conditions and boundary conditions oppose each other, which highlights the complex interplay between the control variables during the data assimilation process. This situation in not unusual and has been observed in other regions (Moore et al., 2011c; Moore et al, 2015).

The rms over all cycles indicates that on average, the initial conditions contribute more than the boundary conditions to ΔI across 40.5°N, while the impact of increments in the surface forcing is generally small.

The contribution of each observing platform to the total transport increment ΔI during each 4D-Var cycle is shown in Fig. 6a. For reference, the percentage number of observations from each different platform during every cycle is shown in Fig. 6b. During a typical cycle, almost 93% of the total number of observations take the form of HF radar data, 5% are satellite SST (daily) and 2% gridded satellite SSH (daily), so HF radar data constitute the largest fraction of all available observations.

While on average, HF radar data together with satellite SSH are the dominant observation platforms controlling ΔI, Fig. 6a reveals that the situation varies from cycle to cycle. For instance, the impact of SSH observations on ΔI appears to be greatest at the beginning of the experiment in the October month even though the number of SSH observations per cycle is constant throughout the experiment. The large impact of the SSH observations is consistent with the significant role that the boundary conditions increments play in controlling the transport (Fig. 5), and this further confirms that the control vector and observation impact calculations are a useful way for monitoring the performance of the data assimilation system as well as quantifying the impact of the observations on the circulation estimates. Also, the impact of HF radar observations on ΔI is almost always prevalent during all cycles and is very significant, despite the relatively small area in which these observations are located.

Fig. 6a shows that on average, SSH and HF radar observations exert approximately the same impact on ΔI. The contribution of each observation platform to the components of ΔI associated with each of the control variable increments of Fig. 5 are qualitatively similar to Fig. 6a (not shown).

Through the study of the alongshore transport of surface water across the single section, we were able to assess that the model is able to reproduce in a rather consistent way, the value of northward transport (Fig. 4a).

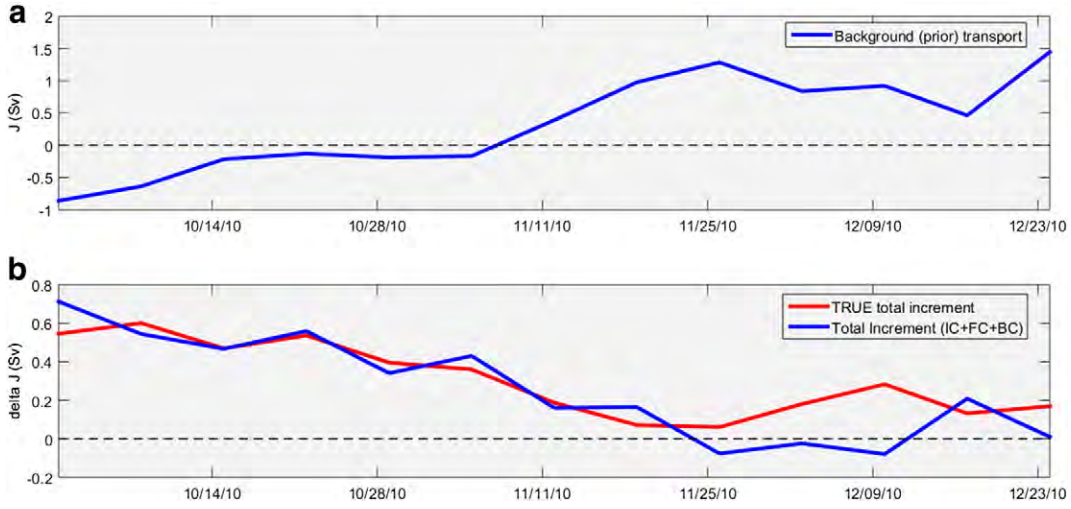

Fig. 4. (a) Time series of the 7-day average background (prior) transport across 40.5°N. Time series of the analysis (posterior) transport increments are shown in (b) across 40.5°N. The red curve represents the transport increments computed directly from the analysis and background circulation estimates of NLROMS, while the blue curve shows the increments computed using the tangent linear assumption.

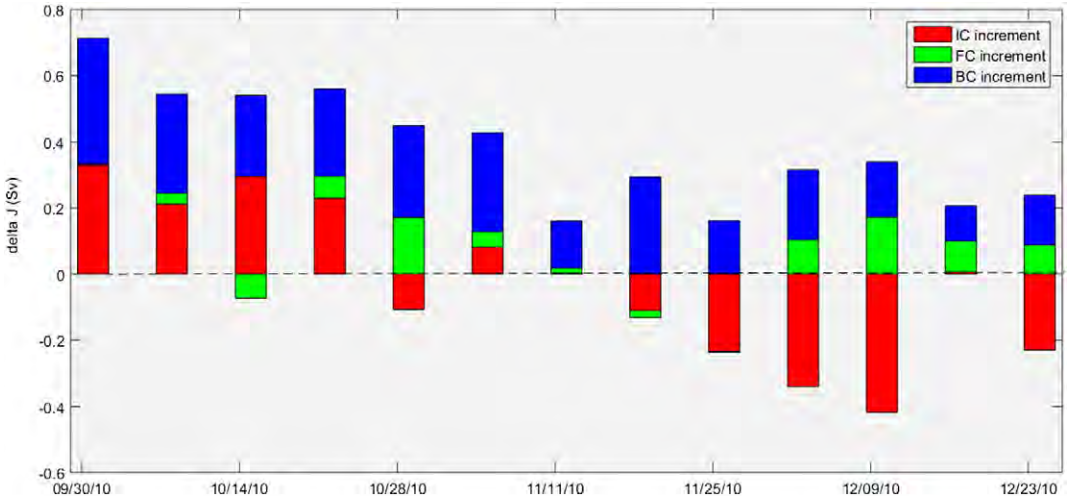

Fig. 5. Time series of the contributions of the 4D-Var increments in the initial conditions, surface forcing, and open boundary conditions to ΔI at 40.5°N.

These results are in accordance to Astraldi et al. (1990), who demonstrated a northward seasonal transport in the central–northern Tyrrhenian Sea with values ranging from 1.4 Sv in winter to 0.2 Sv in summer.

To generalize the results, a second target area was considered comprising the coastal area of GoN and surroundings where data assimilation has the major impact (Fig. 3). Specifically, we consider the average transport of an intermediate watermass, between 300 and 600 m depth which is synonymous with LIW.

As already noted, the transport of such intermediate water in the coastal region of the model domain can be considered as an important aspect of the circulation in that area (Astraldi and Gasparini, 1994; Pierini and Simioli, 1998).

The 7-day average meridional transport between 300 and 600 m across the target area indicated in Fig. 1 was considered and used as a new diagnostic variable to quantify the impact of satellite and HF radar data on the circulation resulting from data assimilation.

Also in this case, the two time series of the transport increment $\Delta I = I_a - I_b$ during each assimilation cycle given by NLROMS and the tangent linear assumption generally agree well during most of the time period, indicating that the tangent linear assumption is valid during each 7-day assimilation cycle (now shown).

After decomposed the transport increments of the LIW water mass into the individual contributions from the 4D-Var control variable increments for the initial conditions, surface forcing and open boundary conditions, the time series of the individual contributions to ΔI are shown in Fig. 7 for each 4D-Var cycle.

Fig. 7 shows that the increments in the initial conditions dominate for the entire duration of the experiment and undoubtedly they are the primary factor controlling ΔI in the coastal area of GoN and surroundings.

In contrast to the previous case, the increments due to boundary conditions play a fairly minor role in controlling LIW transport. The LIW target area is more remote from the open boundaries than the previous domain-wide transport section which probably accounts for the lack of sensitivity to the open boundary conditions. This is also a clear indication that the boundary conditions provided from the coarse model are not sufficient to ensure the proper coupling with the regional model. Hence the need for data assimilation directly in the high-resolution model, as noted earlier.

In Fig. 8, the contribution of each observing platform to the total transport increment ΔI during each 4D-Var cycle is shown for the LIW metric.

Also in this case, it can be seen that, on average, HF radar data together with satellite SSH are the dominant observation platforms controlling ΔI, even if the situation varies from cycle to cycle as for the domain-wide transport section. The impact of HF radar observations on ΔI is almost always prevalent during all cycles and is very significant, despite the relatively small area in which these observations are located.

Fig. 8 also indicates that SST observations have a large impact on ΔI compared to the case of a domain-wide section (Fig. 6).

3.3. Vertical structure

Hydrographic observations of temperature and salinity collected through CTD samplings were used to evaluate the impact of the assimilation on subsurface and deep layers.

The CTD data were collected during the oceanographic cruise TYR01 conducted on board the R/V Urania in October and November 2010 (Francesco Bignami, personal communication).

In order to partially side-step the space–time issue of mismatches between the simulated and measured profiles (*i.e.* the CTD profiles represent a point measurement while a model grid element can be thought as a region of about 9 km^2), the four grid points surrounding each sampling point were interpolated to the CTD profile location to obtain a corresponding simulated profile.

The overall impact of the satellite and HF radar data assimilation on reproducing the water column properties was evaluated by comparing the salinity and temperature from free-run and 4D-Var analysis with those collected by CTD during the TYR01 oceanographic cruise.

CTD data were subdivided depending on the area and day of sampling into two different zones: a very wide section including 5 CTD stations which extends offshore for most of the domain for a total of about 125 km (black points in Fig. 1; hereafter TYR section), and another section consisting of 5 CTD stations extending offshore from the interior of the GoN for about 60 km (red points in Fig. 1; hereafter GON section).

One of the interesting questions raised by data assimilation in a coastal region is how sensitivity spreads from the surface to the rest of the domain. The sensitivity can propagate as free waves (internal waves, Rossby waves, and topographically trapped waves, such as coastally trapped waves) in addition to advection by existing flows (Hoteit et al., 2009).

As the integration of the adjoint model proceeds backward in time, the sensitivity spreads out horizontally away from the observed region and shows obvious interactions with the depth, also far away from the observation region.

The vertical sections show how information is being transferred from the surface via the vertical correlations and the dynamics and how the subsurface density perturbations produce surface pressure

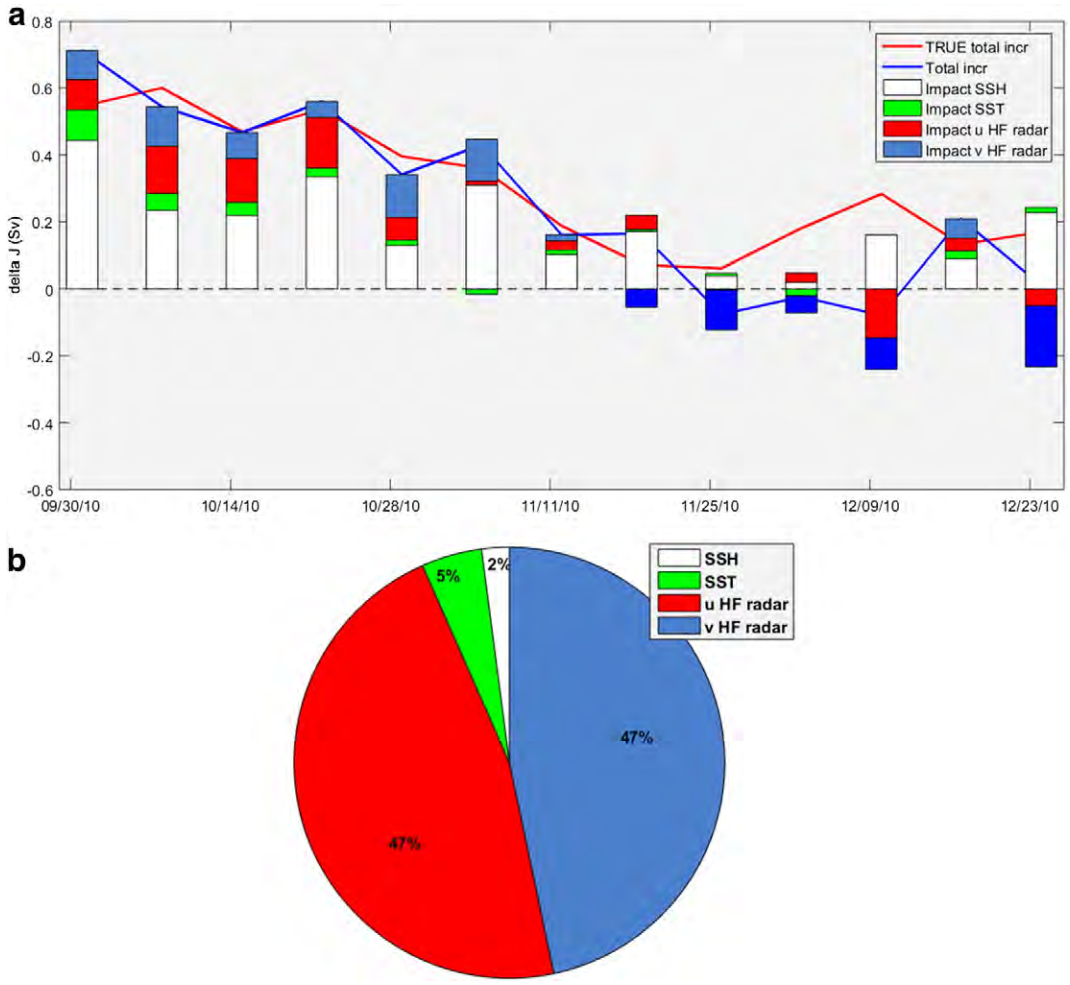

Fig. 6. (a) Time series of the total transport increment ΔI at 40.5°N where the colored bars indicate the contribution of each observing platform during individual 4D-Var cycles. (b) A pie chart of the number of observations that were assimilated during each 4D-Var cycle.

gradients, and the gradients modify surface currents and temperature, according to the momentum equations.

Major improvements were not expected in terms of vertical profiles because no profile data were assimilated in the analyses. Therefore, the corrections in the vertical structure of the water column are only a function of the SSH and SST corrections and their covariance with T and S vertical profiles, as prescribed by the vertical background error covariance matrix.

By comparing single T-S profiles with those from the model, the general shape of the profile is normally quite well reproduced by the ROMS

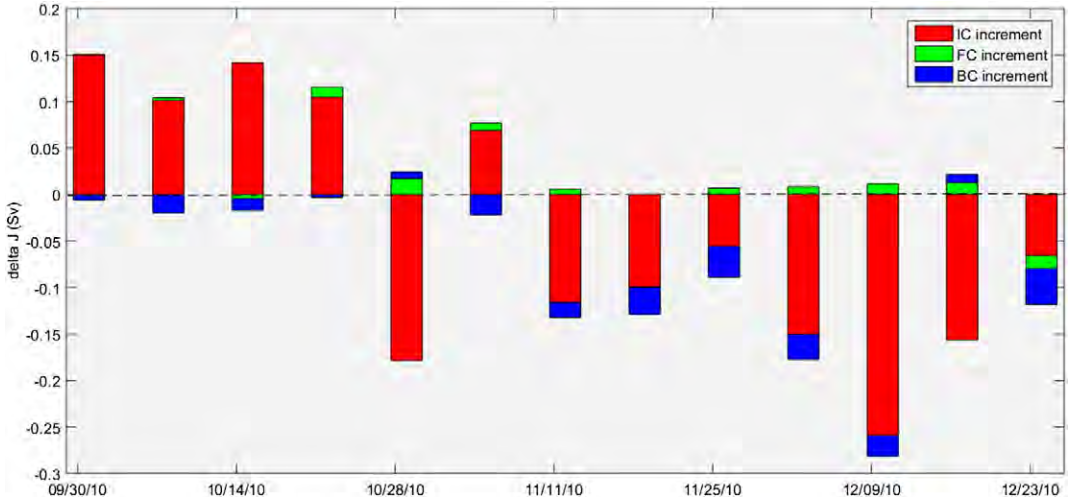

Fig. 7. Time series of the contributions of the 4D-Var increments in the initial conditions, surface forcing, and open boundary conditions to the average transport of the intermediate water mass LIW in the coastal area of GoN and surroundings.

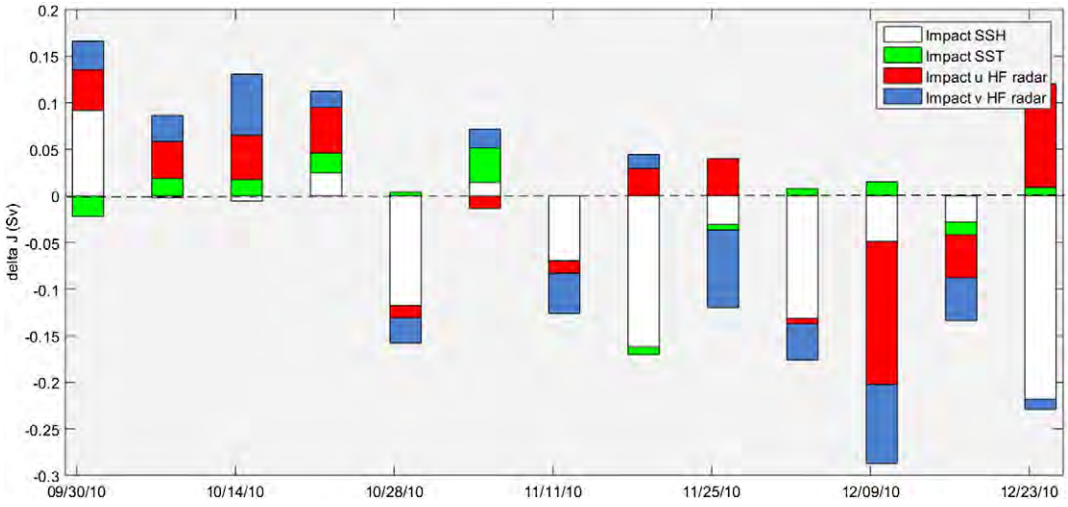

Fig. 8. Time series of the average transport increment ΔI of the intermediate water mass LIW, where the colored bars indicate the contribution of each observing platform during individual 4D-Var cycles.

model and also improved in the 4D-var experiment as it can be seen in Fig. 9. The illustrated individual profile is chosen from the TYR section and represents its second station (13° 37′ 2.3″–39° 42′ 28.8″); it is characterized by a maximum depth of 2700 m of which only the first 500 m are shown (Fig. 9).

The model solution is improved by the assimilation of surface data above all for temperature profile (green line in left panel of Fig. 9). It is observed as the surface temperature decreases by more than 1 °C in the 4D-Var analysis experiment compared to the free-run experiment and clearly it correctly reproduces the measured values (black line). Furthermore, the 4D-Var experiment is able to reproduce the thermocline much better than the free-run experiment while at greater depths it doesn't highlight particular differences respect to free-run experiment.

On the contrary, the 4D-Var analysis experiment shows very slight improvements in salinity (right panel of Fig. 9). The main problem seems to be a systematic bias in the salinity maximum of 38.7 psu, which is systematically underestimated by both the free-run and analysis simulations, even if in the analysis the salinity range is wider, reaching higher and more realistic maxima. In particular for the first 50 m of the profile, it can be seen that both the analysis and the free-run experiments fail to reproduce both the surface values and the subsurface decrement.

At greater depths, no significant difference between the analysis and free-run experiments can be found for the salinity.

The shape of analyzed sections is generally improved by the satellite and HF radar data assimilation, in some cases in a very significant way as can be observed in the Figs. 10–12.

Figs. 10 and 11 show both the field and RMSE comparison between modeled profiles of free-run and analysis experiments and CTD observations (temperature and salinity) for TYR section.

The layers between 20 and 100 m are the most critical, as usual for oceanographic models: at these depths, we found the largest vertical gradients both in T and S. However, the RMSE does not exceed 0.045 °C for temperature (Fig. 10b) and 3×10^{-3} psu in salinity (Fig. 11b) both in free-run and analysis experiment.

Furthermore, the most evident improvement in salinity is related to the correct reproduction of the subsurface salinity increment by the 4D-Var analysis, neglected in the free-run experiment. It is noteworthy that the aforementioned improvement by data assimilation are localized only at deepest stations of the section (while for the mid-depth stations there is little improvement in salinity by the 4D-Var analysis) (Fig. 11 a–b).

Fig. 12 (*a* and *b*) shows the temperature field and RMSE comparisons between the modeled profiles of the free-run and analysis experiments and CTD observations for GON section.

Along this section, the assimilation of surface data generates a substantial improvement in the modeled solution and in the reproduction of temperature section. In particular, the 4D-Var analysis is able to improve the reproduction of thermocline respect to the free-run experiment, even if the thermocline location in the CTD measurement appears localized between 50 and 70 m, while in the analysis and in the free-run, it appears deeper (Fig. 12a). In particular, the analysis experiment is able to reproduce the minimum of temperature above

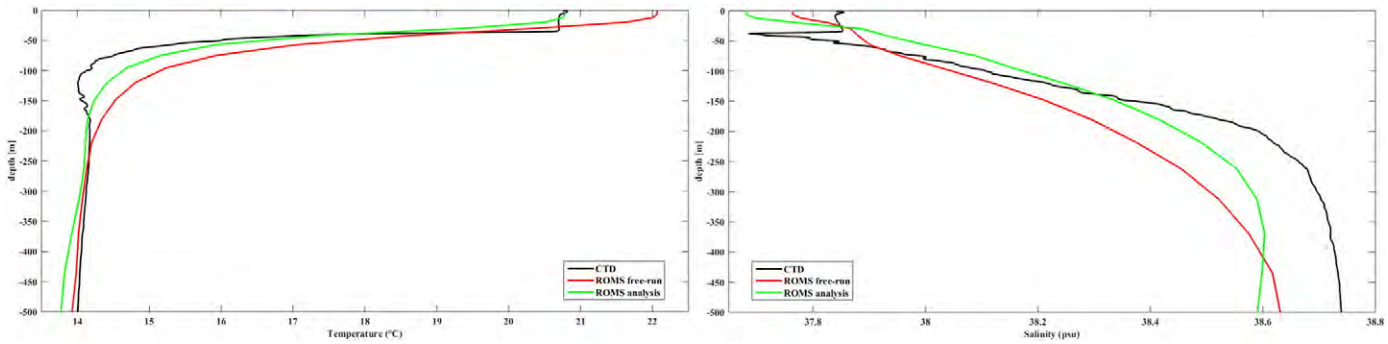

Fig. 9. Temperature (left) and salinity (right) profiles for free-run (red), analysis (green) and CTD (black) for a single station (13° 37′ 2.3″–39° 42′ 28.8″) of TYR section.

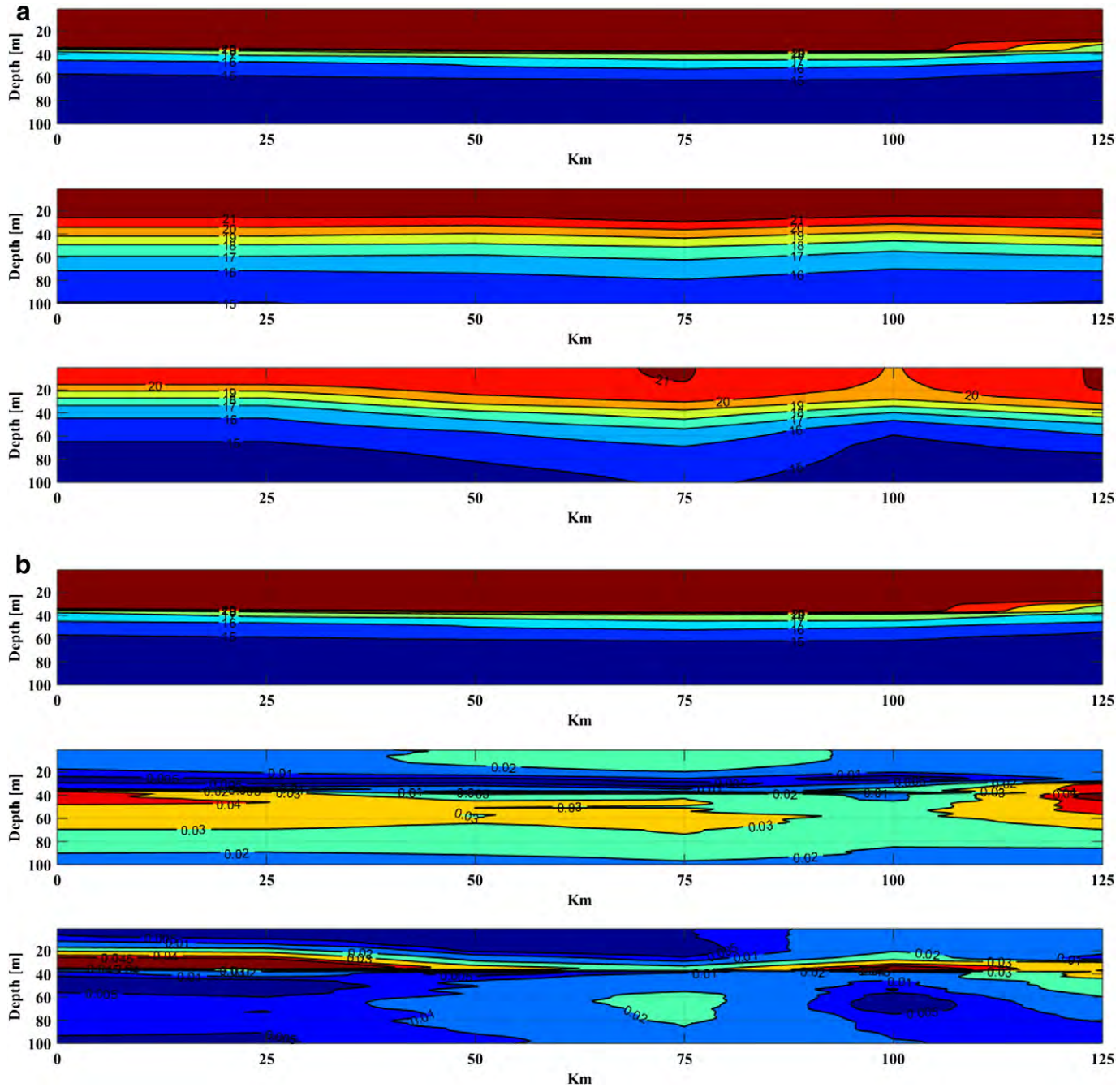

Fig. 10. *a*: Temperature comparison between CTD measurements collected along the TYR section (upper panel), free-run (central panel), and analysis (lower panel) simulations. The locations of CTD stations are shown in the reference map of Fig. 1. *b*: RMSE comparison between modeled profiles and CTD observations of temperature along the TYR section. In the upper panel the CTD measurements, in the central and lower panels the RMSE of free-run and analysis experiments, respectively. The locations of CTD stations are shown in the reference map of Fig. 1.

100 m in almost all stations of GoN section which was absent in the free-run experiment (Fig. 12a).

Also in this case, the RMSE does not exceed the 0.04 °C in a small central area of the section (Fig. 12b). In particular, in the second half of the section corresponding within the GoN, there is a noticeable reduction of error from 0.05 °C in the free-run to 0.01 °C in the 4D-Var analysis experiment. At the two stations inside the GoN, the errors are confined mainly to the upper 50 m in the analysis while in the free-run they extend to 100 m, a clear sign of the effect of the influence of HF radar observations.

Along the GON section, the distribution of salinity follows more or less what was noted above for the TYR section (not shown).

Summarizing, the vertical sections are generally improved by the data assimilation (see Figs. 10–12), and in particular for temperature in a very significant way, even if salinity RMSE appears to be increasing on the surface and the first 50 m.

It is possible that the present set-up tends to dissipate too much the minima of salinity by exaggerating diffusion and/or as a result of SSH assimilation, as noted previously by Olita et al. (2012; 2013).

The impact of data assimilation on the vertical structure deserves further attention: in particular with respect to the background error covariance, and making use of a larger in situ dataset for the validation of vertical profiles.

4. Summary and conclusions

The objective of the present study was to apply and evaluate the effects of 4D-Var data assimilation in a regional model of the southern

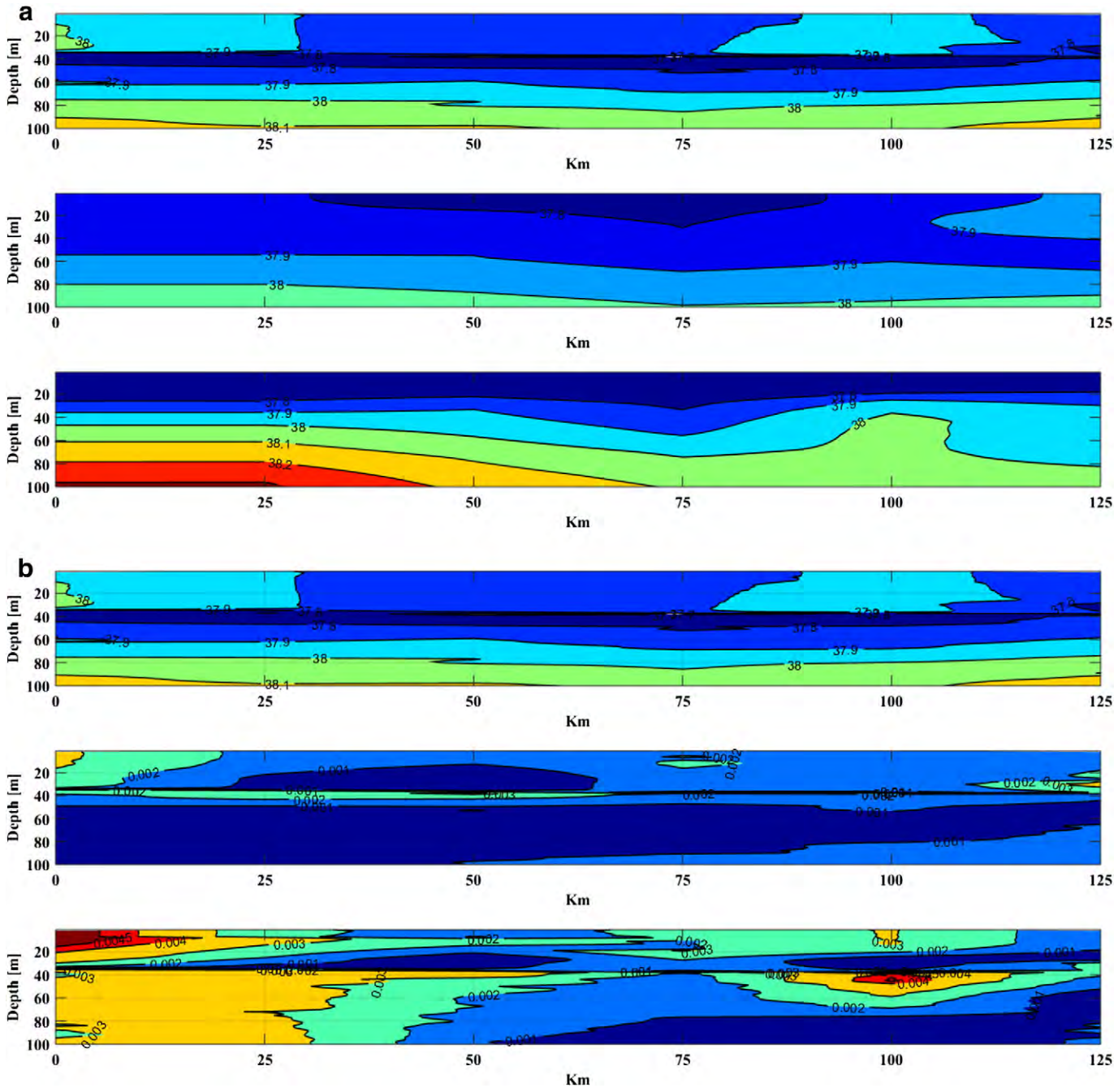

Fig. 11. *a*: Salinity comparison between CTD measurements collected along the TYR section (upper panel), free-run (central panel), and analysis (lower panel) simulations. The locations of CTD stations are shown in the reference map of Fig. 1. *b*: RMSE comparison between modeled profiles and CTD observations of salinity along the TYR section. In the upper panel, the CTD measurements, in the central and lower panels, the RMSE of free-run and analysis experiments, respectively. The locations of CTD stations are shown in the reference map of Fig. 1.

Tyrrhenian Sea using different types of data at high spatial and temporal resolution.

The ocean circulation in the coastal area of the Gulf of Naples and in the southern Tyrrhenian Sea was simulated by applying 4D-Var to long-term observational time series of current velocity data (HF radar), satellite sea surface height and surface temperature measurement within a high-resolution configuration of ROMS.

By assimilating surface currents and satellite data, and comparing model results to output obtained without assimilation, we were able to quantify the impact of different data sources also on different depths that were not directly constrained by assimilation.

In this study, we focused our attention on measures of the alongshore transport that is strongly controlled by the northward winter circulation in the study area and we explored the impact of the observations on a transport metric.

During 4D-Var, the observations are used to correct for uncertainties in the model control variables, namely, the initial conditions, surface forcing, and open boundary conditions.

For instance, results presented here demonstrate that weekly analyses of the alongshore transport along the coastal region are influenced primarily by uncertainties in the initial conditions and only secondarily in the boundary conditions. There is, however, considerable variability from one assimilation cycle to the next, with the initial condition increments dominating almost entirely throughout the experiment.

The majority of the observations available during any given analysis cycle are from HF radar, and on average, these data exert the largest

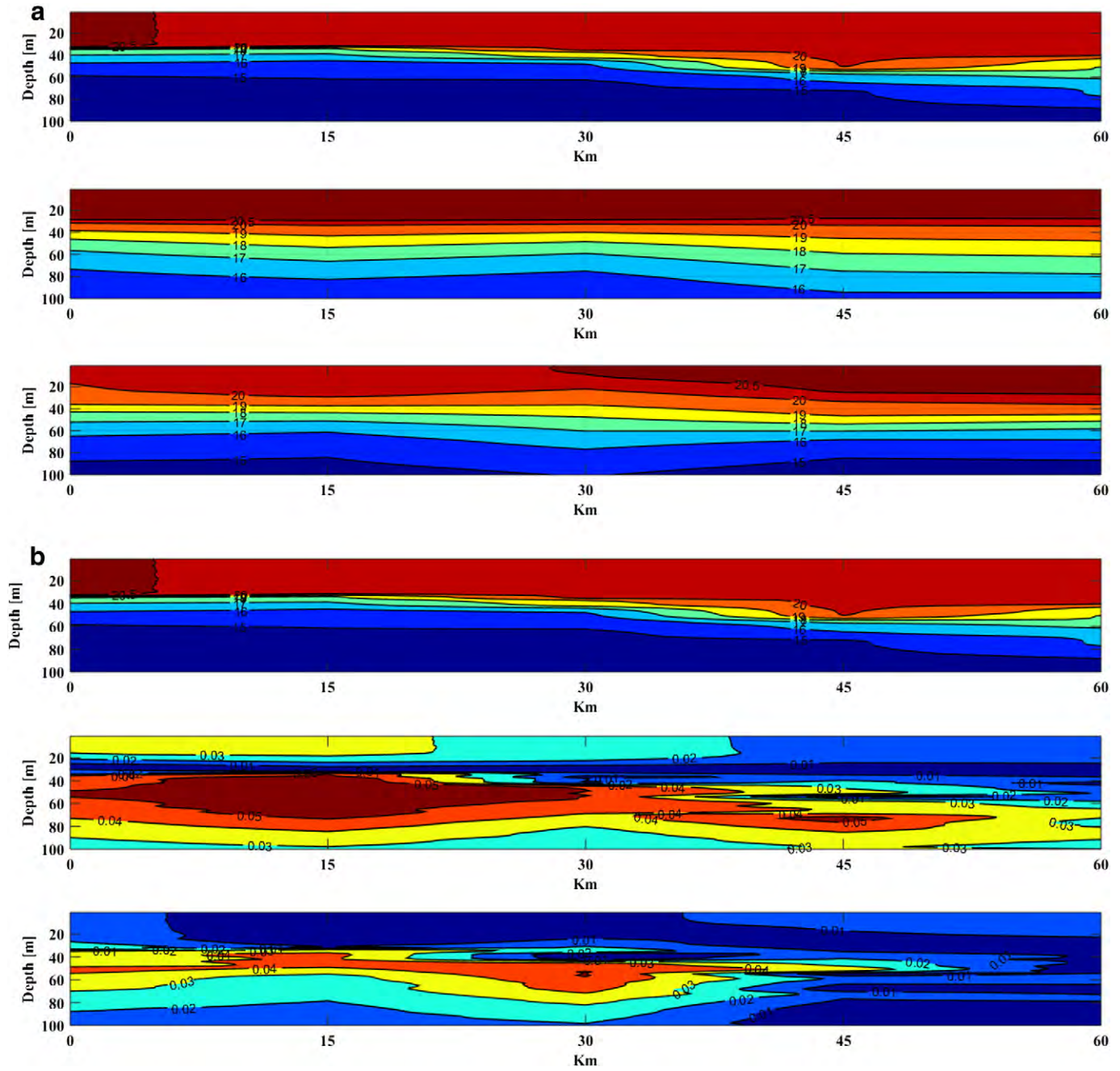

Fig. 12. *a*: Temperature comparison between CTD measurements collected along the GON section (upper panel), free-run (central panel), and analysis (lower panel) simulations. The locations of CTD stations are shown in the reference map of Fig. 1. *b*: RMSE comparison between modeled profiles and CTD observations of temperature along the GON section. In the upper panel, the CTD measurements, in the central and lower panels, the RMSE of free-run and analysis experiments, respectively. The locations of CTD stations are shown in the reference map of Fig. 1.

controlling influence on the coastal transport during both the analysis and forecast cycle. Also, observations from satellite platforms in the form of SSH and, secondly, SST have a considerable impact on analyses of coastal transport, even though these observations represent a relatively small fraction of the available data at any particular time.

The quality of the analysis was evaluated by considering an intercomparison of a free-run and the 4D-Var analysis with an observational dataset comprising (a) synoptic satellite images for the detection of mesoscale features and qualitative comparison with simulations and (b) independent salinity and temperature profiles, collected at the end of October 2010.

The assimilation of satellite and HF radar data brings to bear important improvements in the simulation of the circulation in the GoN and southern Tyrrhenian Sea area.

In particular, 4D-Var data assimilation can recover some of the dynamical features and it is able to correct submesoscale circulation features in the form of squirts and jets along the GoN and its northern coastal area.

The impact of the satellite and HF radar data assimilation on the vertical structure is also evidenced and can be understood in terms of wave dynamics and changes in large-scale pressure gradients, while the more local influences are most likely associated with horizontal advection.

In the vertical, both salinity and temperature profiles are improved by the data assimilation in terms of RMSE even if the layers between 20 and 100 m are the most critical, as usual for oceanographic models because at these depths we found the largest vertical gradients both in T and S.

At these depths, however, the RMSE does not exceed 0.04 °C for temperature and 2×10^{-3} psu in salinity both in free-run and analysis experiment.

Considering that no TS profiles have been assimilated in the analyses, it is clear that the quality of the analyses in the vertical is only a function of the vertical background error covariances.

Therefore, to fix the questionable impact of the surface data on the vertical structure, future work focus on improving the background error covariances, and on the assimilation of vertical profiles data.

The limited set of experiments presented represent preliminary tests of the assimilation system, and much remains to be done. Further work is needed to adjust the weight and balance of the various controls, which ought to improve the dynamics of the assimilation results. In addition, the data assimilated ought to be complemented also with other types of observations such as subsurface observations which, even though typically few in number compared to satellite observations, can have a considerable and important influence on the analysis and forecast circulations.

Finally, we note that both the control vector and the observation impact calculations are a useful way for monitoring the performance of the data assimilation system, as well as quantifying the impact of the observations on the circulation estimates.

However, the experiments presented here emphasize the importance and significance of HF radar data assimilation in high-resolution numerical ocean models and suggest that the ROMS/4D-Var system is feasible for coastal area applications.

The present study demonstrates the potential applications of highly innovative methodologies and instrumentation in order to better assess the surface circulation, with possible feedbacks on the understanding of transport processes in critical coastal areas, thus addressing issues of national and Mediterranean importance.

Acknowledgments

This work has been funded by the Flagship Project RITMARE – The Italian Research for the Sea – coordinated by the Italian National Research Council and funded by the Italian Ministry of Education, University and Research within the National Research Program 2011-2013, by the FP7 PERSEUS Project, by the EU MED TOSCA Project.

References

Anderson, D.L.T., Sheinbaum, J., Haines, K., 1996. Data assimilation in ocean models. Rep. Prog. Phys. 59, 1209–1266.

Astraldi, M., Gasparini, G.P., 1994. The seasonal characteristics of the circulation in the Tyrrhenian Sea. In: La Violette, P. (Ed.), Seasonal and Interannual Variability of the Western Mediterranean SeaCoastal and Estuarine Studies vol. 46. American Geophysical Union, pp. 115–134.

Astraldi, M., Gasparini, G.P., Manzella, G.M.R., Hopkins, T.S., 1990. Temporal variability of currents in the eastern Ligurian Sea. J. Geophys. Res. 95, 1515–1522.

Barth, A., Alvera-Azca´rate, A., Weisberg, R., 2008. Assimilation of high-frequency radar currents in a nested model of the West Florida Shelf. J. Geophys. Res. Oceans 113 (c8) (1-C08,033).

Bellomo, L., Griffa, A., Cosoli, S., Falco, P., Gerin, R., Iermano, I., Kalampokis, A., Kokkini, Z., Lana, A., Magaldi, M.G., Mamoutos, I., Mantovani, C., Marmain, J., Potiris, E., Sayol, J.M., Barbin, Y., Berta, M., Borghini, M., Bussani, A., Corgnati, L., Dagneaux, Q., Gaggelli, J., Guterman, P., Mallarino, D., Mazzoldi, A., Molcard, A., Orfila, A., Poulain, P.-M., Quentin, C., Tintoré, J., Uttieri, M., Vetrano, A., Zambianchi, E., Zervakis, V., 2015. Toward an integrated HF radar network in the Mediterranean Sea to improve search and rescue and oil spill response: the TOSCA project experience. J. Oper. Oceanogr. http://dx.doi.org/10.1080/1755876X.2015.1087184.

Bennett, A.F., 2002. Inverse Modeling of the Ocean and the Atmosphere. Cambridge Univ. Press, New York.

Breivik, Ø., Saetra, Ø., 2001. Real time assimilation of HF radar currents into a coastal ocean model. J. Mar. Syst. 28 (3), 161–182.

Broquet, G., Edwards, C.A., Moore, A.M., Powell, B.S., Veneziani, M., Doyle, J.D., 2009a. Application of 4D-variational data assimilation to the California current system. Dynam. Atmos. Oceans. 48, 69–91.

Broquet, G., Moore, A.M., Arango, H.G., Edwards, C.A., Powell, B.S., 2009b. Ocean state and surface forcing correction using the ROMS-IS4DVAR data assimilation system. Mercator Ocean Q. Newsl. 34, 5–13.

Broquet, G., Moore, A.M., Arango, H.G., Edwards, C.A., 2011. Corrections to ocean surface forcing in the California current system using 4D-variational data assimilation. Ocean Model. 36, 116–132.

Buffoni, G., Falco, P., Griffa, A., Zambianchi, E., 1997. Dispersion processes and residence times in a semi-enclosed basin with recirculating gyres: an application to the Tyrrhenian sea. J. Geophys. Res. Oceans. 102, 18699–18713.

Chao, Y., Li, Z., Farrara, J., McWilliams, J.C., Bellingham, J., Capet, X., Chavez, F., Choi, J.-K., Davis, R., Doyle, J., Fratantoni, D.M., Li, P., Marchesiello, P., Moline, M.A., Paduan, J., Ramp, S., 2009. Development, implementation and evaluation of a data-assimilative ocean forecasting system off the central California coast. Deep Sea Res. Part II 56, 100–126.

Chapman, D.C., 1985. Numerical treatment of cross-shelf open boundaries in a barotropic coastal ocean model. J. Phys. Oceanogr. 15, 1060–1075.

Cianelli, D., Falco, P., Iermano, I., Mozzillo, P., Uttieri, M., Buonocore, B., Zambardino, G., Zambianchi, E., 2015. Inshore/offshore water exchange in the Gulf of Naples. J. Mar. Syst. 145, 37–52.

Corgnati, L., Mantovani, C., Griffa, A., Forneris, V., Tronconi, C., Santoleri, R., Cosoli, S., Serafino, F., Raffa, F., Uttieri, M., Kalampokis, A., Zambianchi, E., 2015. The RITMARE Italian coastal radar network: operational system and data interoperability framework. Proc. of the 7th EuroGOOS Conference (in press).

Daescu, D.N., 2008. On the sensitivity equations for four-dimensional variational (4D-Var) data assimilation. Monthly Weather Rev. 136, 3050–3065.

Dee, D.P., Uppala, S.M., Simmons, A.J., Berrisford, P., Poli, P., Kobayashi, S., Andrae, U., Balmaseda, M.A., Balsamo, G., Bauer, P., Bechtold, P., Beljaars, A.C.M., van de Berg, L., Bidlot, J., Bormann, N., Delsol, C., Dragani, R., Fuentes, M., Geer, A.J., Haimberger, L., Healy, S.B., Hersbach, H., Hólm, E.V., Isaksen, L., Kållberg, P., Köhler, M., Matricardi, M., McNally, A.P., Monge-Sanz, B.M., Morcrette, J.-J., Park, B.-K., Peubey, C., de Rosnay, P., Tavolato, C., Thépaut, J.-N., Vitart, F., 2011. The ERA-Interim reanalysis: configuration and performance of the data assimilation system. Q. J. R. Meteor. Soc. 137 (656), 553–597.

Dombrowsky, E., Bertino, L., Brassington, G.B., Chassignet, E.P., Davidson, F., Hurlburt, H.E., Kamachi, M., Lee, T., Martin, M.J., Mei, S., Tonani, M., 2009. GODAE systems in operation. Oceanography 22, 80–95. http://dx.doi.org/10.5670/oceanog.2009.68.

Fairall, C.W., Bradley, E.F., Rogers, D.P., Edson, J.B., Young, G.S., 1996. Bulk parameterization of air-sea fluxes for tropical ocean-global atmosphere Coupled-Ocean Atmosphere Response Experiment. J. Geophys. Res. 101, 3747–3764.

Flather, R.A., 1976. A tidal model of the northwest European continental shelf. Memoires de la Societe Royale de Sciences de Liege 6, pp. 141–164.

Gelaro, R., Zhu, Y., 2009. Examination of observation impacts derives from observing system experiments (OSEs) and adjoint models. Tellus 61A, 179–193.

Gopalakrishnan, G., Blumberg, A.F., 2012. Assimilation of HF radar-derived surface currents on tidal-timescales. J. Oper. Oceanogr. 5, 75–87.

Grieco, L., Tremblay, L.B., Zambianchi, E., 2005. A hybrid approach to transport processes in the Gulf of Naples: an application to phytoplankton and zooplankton population dynamics. Cont. Shelf Res. 25 (5), 711–728.

Gürol, S., Weaver, A.T., Moore, A.M., Piacentini, A., Arango, H.G., Gratton, S., 2013. B preconditioned minimization algorithms for variational data assimilation with the dual formulation. Q. J. R. Meteorol. Soc. http://dx.doi.org/10.1002/qj.2150.

Haidvogel, D.B., Arango, H.G., Hedstrom, K., Beckmann, A., Malanotte-Rizzoli, P., Shchepetkin, A.F., 2000. Model evaluation experiments in the North Atlantic Basin: simulations in nonlinear terrain-following coordinates. Dyn. Atmos. Oceans 32, 239–281.

Hoteit, I., Köhl, A., 2006. Efficiency of reduced-order, time-dependent adjoint data assimilation approaches. J. Oceanogr. 62, 539–550.

Hoteit, I., Cornuelle, B., Kim, S.Y., Forget, G., Kohl, A., Terrill, E., 2009. Assessing 4D-VAR for dynamical mapping of coastal high-frequency radar in San Diego. Dyn. Atmos. Oceans 48, 175–197.

Iermano, I., Liguori, G., Iudicone, D., Buongiorno Nardelli, B., Colella, S., Zingone, A., Saggiomo, V., Ribera d'Alcalà, M., 2012. Filament formation and evolution in buoyant coastal waters: Observation and modelling. Prog. Oceanogr. 106, 118–137. http://dx.doi.org/10.1016/j.pocean.2012.08.003.

Janekovic, I., Powell, B.S., Matthews, D., McManus, M.A., Sevadjian, J., 2013. 4D-Var data assimilation in a nested, coastal ocean model: A Hawaiian case study. J. Geophys. Res. Oceans 118, 1–14.

Köhl, A., Stammer, D., 2004. Optimal observations for variational data assimilation. J. Phys. Oceanogr. 34, 529–542.

Korres, G., Nittis, K., Hoteit, I., Triantafyllou, G., 2009. A high resolution data assimilation system for the Aegean Sea hydrodynamics. J. Mar. Syst. 77, 325–340.

Krivosheya, V.G., Ovchinnikov, I.M., 1973. Properties of the geostrophic circulation of the Tyrrhenian Sea. Oceanology 13, 996–1002.

Kurapov, A., Egbert, G., Allen, J., Miller, R., Erofeeva, S., Kosro, P., 2003. The M 2 internal tide off Oregon: Inferences from data assimilation. J. Phys. Oceanogr. 33 (8), 1733–1757.

Kurapov, A., Egbert, G., Allen, J., Miller, R., 2009. Representer-based analyses in the coastal upwelling system. Dyn. Atmos. Oceans 48, 198–218.

Kurapov, A., Foley, D., Strub, P.T., Egbert, G., Allen, J., 2011. Variational assimilation of satellite observations in a coastal ocean model off Oregon. J. Geophys. Res. 116, C05006.

Langland, R.H., Baker, N.L., 2004. Estimation of observation impact using the NRL atmospheric variational data assimilation adjoint system. Tellus 56A, 189–201.

Lellouche, J.-M., Le Galloudec, O., Drévillon, M., Régnier, C., Greiner, E., Garric, G., Ferry, N., Desportes, C., Testut, C.-E., Bricaud, C., Bourdallé-Badie, R., Tranchant, B., Benkiran, M., Drillet, Y., Daudin, A., De Nicola, C., 2013. Evaluation of global monitoring and forecasting systems at Mercator Océan. Ocean Sci. 9, 57–81. http://dx.doi.org/10.5194/os-9-57-2013.

Lewis, J.K., Shulman, I., Blumberg, A.F., 1998. Assimilation of Doppler radar current data into numerical ocean models. Cont. Shelf Res. 18, 541–559.

Li, Z., Chao, Y., McWilliams, J.C., Ide, K., 2008. A three-dimensional variational data assimilation scheme for the Regional Ocean Modeling System: Implementation and basic experiments. J. Geophys. Res. 113 (C2), C05002.

Menna, M., Mercatini, A., Uttieri, M., Buonocore, B., Zambianchi, E., 2007. Wintertime transport processes in the Gulf of Naples investigated by HF radar measurements of surface currents. Nuovo Cimento-C 30 (6), 605–622.

Millot, C., 1987. Circulation in the western Mediterranean Sea. Oceanol. Acta 10, 143–149.
Moore, A.M., Arango, H.G., Broquet, G., Powell, B.S., Weaver, A.T., Zavala-Garay, J., 2011a. The Regional Ocean Modeling System (ROMS) 4-dimensional variational data assimilation systems: Part I – System overview and formulation. Prog. Oceanogr. 91 (1), 34–49.
Moore, A.M., Arango, H.G., Broquet, G., Edwards, C., Veneziani, M., Powell, B.S., Foley, D., Doyle, J.D., Costa, D., Robinson, P., 2011b. The Regional Ocean Modeling System (ROMS) 4-dimensional variational data assimilation systems: Part II – Performance and application to the California Current System. Prog. Oceanogr. 91 (1), 50–73.
Moore, A.M., Arango, H.G., Broquet, G., Edwards, C., Veneziani, M., Powell, B.S., Foley, D., Doyle, J.D., Costa, D., Robinson, P., 2011c. The Regional Ocean Modeling System (ROMS) 4-dimensional variational data assimilation systems: Part III – Observation impact and observation sensitivity in the California Current System. Prog. Oceanogr. 91 (1), 74–94.
Moore, et al., 2015. Observing System Impacts on Estimates of California Current Transport. In: Liu, Yonggang, Kekering, Heather, Weisberg, Robert (Eds.), Coastal Ocean Observing Systems. Elsevier, pp. 351–369 (Chapter 19).
Oke, P.R., Allen, J.S., Miller, R.N., Egbert, G.D., Kosro, P.M., 2002. Assimilation of surface velocity data into a primitive equation coastal ocean model. J. Geophys. Res. 107, 3122.
Olita, A., Dobricic, S., Ribotti, A., Fazioli, L., Cucco, A., Dufau, C., Sorgente, R., 2012. Impact of sla assimilation in the Sicily channel regional model: model skills and mesoscale features. Ocean Sci. 8 (4), 485–496.
Olita, A., Ribotti, A., Fazioli, L., Perilli, A., Sorgente, R.R., 2013. Surface circulation and upwelling in the western Sardinia sea: A numerical study. Cont. Shelf Res. 71, 95–108.
Paduan, J.D., Shulman, I., 2004. HF radar data assimilation in the Monterey Bay area. J. Geophys Res. 109, C07S09.
Paduan, J.D., Washburn, L., 2013. High-frequency radar observations of ocean surface currents. Annu. Rev. Mar. Sci. 5, 1,115–1,136.
Pierini, S., Simioli, A., 1998. A wind-driven circulation model of the Tyrrhenian Sea area. J. Mar. Syst. 18 (1), 161–178.
Pinardi, N., Coppini, G., 2010. Preface "Operational oceanography in the Mediterranean Sea: the second stage of development". Ocean Sci. 6, 263–267. http://dx.doi.org/10.5194/os-6-263-2010.
Poulain, P.M., Zambianchi, E., 2007. Surface circulation in the central Mediterranean Sea as deduced from Lagrangian drifters in the 1990s. Cont. Shelf Res. 27 (7), 981–1001.
Powell, B.S., Arango, H.G., Moore, A.M., Di Lorenzo, E., Milliff, R.F., Foley, D., 2008. 4DVAR data assimilation in the Intra-Americas Sea with the Regional Ocean Modeling System (ROMS). Ocean Model. 25, 173–188.
Pujol, M.-I., Faugere, Y., Legeais, J.-F., Rio, M.-H., Schaeffer, P., Bronner, E., Picot, N., 2013. A 20-Year Reference Period for SSALTO/DUACS Products (OSTST, 2013).
Rinaldi, E., Buongiorno Nardelli, B., Zambianchi, E., Santoleri, R., Poulain, P.-M., 2010. Lagrangian and Eulerian observations of the surface circulation in the Tyrrhenian Sea. J. Geophys. Res. 115, C04024.
Rio, M.-H., Mulet, S., Picot, N., 2013. New global mean dynamic topography from a GOCE geoid model, altimeter measurements and oceanographic in-situ data. Proceedings of the ESA Living Planet Symposium, Edinburg (September 2013).
Shchepetkin, A.F., McWilliams, J.C., 2003. A method for computing horizontal pressure-gradient force in an oceanic model with a nonaligned vertical coordinate. J. Geophys. Res. 108 (C3), 3090.
Shchepetkin, A.F., McWilliams, J.C., 2005. The Regional Ocean Modeling System: a split–explicit, free-surface, topography following coordinates ocean model. Ocean Model. 9, 347–404.
Shulman, I., Paduan, J.D., 2009. Assimilation of HF radar-derived radials and total currents in the Monterey Bay area. Deep-Sea Res. II 56, 149–160.
Uttieri, M., Cianelli, D., Buongiorno Nardelli, B., Buonocore, B., Falco, P., Colella, S., Zambianchi, E., 2011. Multiplatform observation of the surface circulation in the Gulf of Naples (Southern Tyrrhenian Sea). Ocean Dyn. 61, 779–796.
Vandenbulcke, L., Barth, A., Rixen, M., Alvera-Azcarate, A., Ben Bouallegue, Z., Beckers, J.M., 2006. Study of the combined effects of data assimilation and grid nesting in ocean models – application to the Gulf of Lions. Ocean Sci. 2, 213–222. http://dx.doi.org/10.5194/os-2-213-2006.
Warner, J.C., Sherwood, C.R., Arango, H.G., Signell, R.P., 2005. Performance of four turbulence closure methods implemented using a generic length scale method. Ocean Model. 8, 81–113.
Wilkin, J.L., Arango, H.G., Haidvogel, D.B., Lichtenwalner, C.S., Glenn, S.M., Hedstrom, K.S., 2005. A regional ocean modeling system for the long-term ecosystem observatory. J. Geophys. Res. 110, C06S91.
Yu, P., Kurapov, A.L., Egbert, G.D., Allen, J.S., Kosro, P.M., 2012. Variational assimilation of HF radar surface currents in a coastal ocean model off Oregon. Ocean Model. 49–50, 86–104.
Zhang, W.G., Wilkin, J.L., Arango, H.G., 2010. Towards an integrated observation and modeling system in the New York Bight using variational methods. Part I: 4DVAR data assimilation. Ocean Model 35, 119–133.
Zhu, Y., Gelaro, R., 2008. Observation sensitivity calculations using the adjoint of the gridpoint statistical interpolation (GSI) analysis system. Mon. Weather Rev. 136, 335–351.